Structures 79 (2025) 109419

Contents lists available at ScienceDirect

Structures

journal homepage: www.elsevier.com/locate/structures

Definition of differential seismic input motions for out-of-plane dynamic testing of unreinforced masonry gable walls considering different roof configurations

Michele Mirra [a,*], Nicolò Damiani [b,c], Satyadhrik Sharma [d], Francesco Graziotti [b,c], Francesco Messali [d]

[a] Department of Engineering Structures, Section of Bio-Based Structures and Materials, Delft University of Technology, Stevinweg 1, Delft 2628 CN, the Netherlands
[b] Department of Civil Engineering and Architecture, University of Pavia, Via Ferrata 3, Pavia 27100, Italy
[c] European Centre for Training and Research in Earthquake Engineering - EUCENTRE, via Ferrata 1, Pavia 27100, Italy
[d] Department of Materials, Mechanics, Management & Design, Section of Applied Mechanics, Delft University of Technology, Stevinweg 1, Delft 2628 CN, the Netherlands

ARTICLE INFO

Keywords:
Gable walls
Numerical modelling
Seismic response
Seismic vulnerability
Input motion definition
Timber roof
Unreinforced masonry

ABSTRACT

Unreinforced masonry gables are widely present in low-rise existing buildings and are particularly vulnerable to seismic events, as demonstrated by the several observed out-of-plane collapses of these structural elements during earthquakes. Since the structural behaviour of gable walls has been scarcely investigated in the literature, a large-scale testing programme (ERIES-SUPREME) has been initiated by research institutions in the Netherlands (TU Delft, TNO) and Italy (EUCENTRE, University of Pavia, IUSS Pavia), to dynamically characterise the gable out-of-plane seismic response. Shake-table tests on full-scale masonry gables are being conducted at the 9D LAB facility in EUCENTRE (Pavia, Italy), incorporating the effects of different ground motions, structures and roof stiffnesses. This facility features both a top and a bottom shake table, allowing for separate input motions: therefore, the effect of the roof dynamic behaviour can be accounted for by applying differential signals. This work presents the procedure used to define such input motions. While for tectonic signals direct earthquake recordings at floor level are accessible from existing monitored masonry buildings in Italy, for induced signals in the Netherlands such data are not available. Thus, in the latter case, numerical analyses are conducted considering a reference unreinforced masonry building subjected to induced earthquakes, with three roof configurations representing flexible, semi-flexible, and stiff diaphragms. Based on the obtained outcomes, input signals are derived for both induced and tectonic earthquake scenarios, leading to the final definition of the testing protocol for the ERIES-SUPREME experimental campaign. The findings of this study are also broadly applicable for the derivation of input motions in the planning of benchmark experiments where parts of the structural system cannot be explicitly reproduced due to testing constraints.

1. Introduction

Typical low-rise existing masonry buildings in Europe commonly feature unreinforced masonry (URM) walls, complemented by diverse pitched roof configurations, supported or finished by masonry gables. These structures also form a large part of the building stock for several seismic-prone countries, including areas subject to both natural hazard and human-induced seismicity. In such buildings, the masonry gables are often associated with the highest seismic vulnerability, as extensively documented in past post-earthquake damage assessments worldwide, e.g. in Iran [1], Italy [2–6], Nepal [7,8], New Zealand [9], Turkey [10–19], Croatia [20], Pakistan [21], and China [22]. This vulnerability can be attributed to the large slenderness of masonry gables as well as to their poor connections with the roof diaphragm. Moreover, their positioning at the uppermost part of the building exposes them to amplified seismic excitation in comparison to the ground motion, while being subjected to low values of overburden load. The interaction of gables with flexible roof diaphragms can also contribute to the seismic vulnerability of the gable-roof system, due to the potential further amplification of the seismic motion [23]. However, there are

* Corresponding author.
E-mail addresses: m.mirra@tudelft.nl (M. Mirra), nicolo.damiani@unipv.it (N. Damiani), S.Sharma-9@tudelft.nl (S. Sharma), francesco.graziotti@unipv.it (F. Graziotti), F.Messali@tudelft.nl (F. Messali).

https://doi.org/10.1016/j.istruc.2025.109419
Received 5 November 2024; Received in revised form 8 May 2025; Accepted 9 June 2025
Available online 12 June 2025

very limited experimental data regarding the performance of URM gables, and most of the data come from tests simulating a complete building, which are not specifically focused on these structural elements. Furthermore, dynamic experimental tests are fundamental for investigating the seismic out-of-plane (OOP) capacity of URM gables. While a number of dynamic experimental campaigns have been conducted on rectangular walls [24–31], also exploring the influence of boundary conditions or relative support motions [32–36], only limited research focuses on gables in literature. One notable investigation in this framework was conducted on a complete roof sub-structure, consisting of URM gables resting on a reinforced concrete floor slab and supporting a timber roof, which was incrementally dynamically tested until the OOP collapse of the gables [23]. Another study [37] involved dynamic tests on two scaled specimens made of brick and stone masonry, including a façade with a gable on top and two orthogonal return walls, but neglecting the presence of roof and floor diaphragms. In addition, several experimental investigations have been conducted on URM buildings with gables supporting their roof structures [38–44], but the achieved results are hardly applicable for understanding the seismic OOP capacity of gables: either other failure mechanisms governed the global seismic response of the building and prevented the OOP failure of gables [44], or, even when the failure of roof or gables was preceding any other mechanism, the experiments were terminated before the complete collapse due to safety concerns or potential damage to testing facilities [40].

The inadequate seismic performance of timber roof diaphragms in URM buildings has been often addressed by means of retrofitting measures that might limit the roof in-plane deflections, thus reducing OOP damage of the connected URM walls. Although the substitution of existing timber diaphragms with concrete is still a common practice, it has also been documented to worsen the global seismic performance of the building by locally increasing the mass and stiffness at the top of the structure [3,5,45]. A promising and more sustainable alternative is to employ timber-based strengthening techniques [46–49]. While several experimental and numerical investigations have demonstrated the improvement in the diaphragms' in-plane response by adopting these techniques [42,50–62], their effect on the overall seismic performance of a URM building, and particularly in relation to the gables, remains insufficiently explored.

Within this framework, the ERIES-SUPREME (*Seismic oUt-of-Plane REsponse of Masonry gablEs*) project [63–65] – a joint initiative of Delft University of Technology, the Dutch Organisation for Applied Scientific Research (TNO), EUCENTRE Foundation, IUSS Pavia, and University of Pavia – aims at improving the understanding of the seismic OOP response of URM gables within existing buildings. The first general goal of the project is to produce experimental data on the dynamic behaviour of URM gables, currently missing from published literature. All generated experimental data, along with the associated instrumentation schemes, are openly available for download in a dedicated repository [64], and will be used as benchmark for refining and calibrating existing numerical modelling approaches, or even developing new ones. The force and displacement capacity of URM gables subjected to OOP dynamic loading is being investigated by carrying out incremental dynamic tests, resuming testing from a lower level of seismic intensity after observations of damage are made. A second objective of the project is to quantify the influence of roof diaphragms on the OOP response of URM gables. More specifically, it seeks to determine how the stiffness of the roof structure and the efficiency of its connections to the gables affect their performance at different damage states. These investigations also aim to promote the use of sustainable timber-based seismic retrofitting techniques for roof diaphragms in existing URM constructions, by showing how the increase in stiffness and hysteretic energy dissipation are able to improve the seismic response at gable and whole building level in comparison to less reversible methods, such as the strengthening by means of concrete slabs.

The large-scale experimental campaign within the ERIES-SUPREME project is being conducted at the EUCENTRE facilities in Pavia (Italy), using the recently installed 9D LAB [66]. This innovative seismic testing system (Fig. 1) consists of a top and a bottom shake table, and allows to apply input motions covering nine degrees of freedom, making it possible to reproduce inter-storey displacements occurring during earthquakes. The 9D LAB in-plan dimensions allow for testing a full-scale, 6-m-long and 3-m-high, masonry gable; however, they are not sufficient to accommodate an entire roof structure. As a result, the influence of its stiffness on the seismic OOP response of the gables is accounted for by the input motions imposed to the bottom and top shake tables. The main objective of this study is the derivation of these input accelerograms for tectonic and induced earthquake scenarios, considering three configurations for the roof structure: a flexible (as-built) timber roof, a semi-flexible (timber-retrofitted) roof, and a stiff (concrete) roof. While the effects of both induced and tectonic earthquakes are considered, the distinction between the effects of far-field and near-field earthquakes [67,68] is not addressed in the present study. Input signals at gable level from tectonic earthquakes could be obtained from actual earthquake recordings in existing monitored URM structures in Italy [69,70]; however, this is not the case for regions affected by induced seismicity, such as the Groningen province in the Netherlands [71–73]. Specifically, the floor motions and floor spectra suggested by the current Dutch code NPR 9998 are based on established probabilistic models for larger seismic intensities than those recorded to date [74,75], and do not correspond to past earthquakes. Therefore, to assess how URM buildings typical for the Groningen area filter and amplify such motions up to the roof level, advanced numerical simulations on a reference URM terraced house are performed (Fig. 1). The simulations consider the three aforementioned scenarios – flexible, semi-flexible, stiff – for the roof stiffness.

The input motions are derived following the methodology reported in Section 2. In incremental dynamic testing, the scaling of one or a few ground motions, such as the induced and tectonic earthquakes used in this study, introduces uncertainties in terms of the representativeness of the structural response; therefore, the original motions must be selected to correspond to the intensity level at which the response of interest is most accurately captured. In this context, records corresponding to minor or moderate structural damage (damage states DS2–DS3 [40,44]) have been chosen for the induced seismicity, as higher damage levels are deemed unrealistic for this scenario, while extensive structural damage (damage state DS4 [40,44]) has been selected for the tectonic seismicity to reflect the structural degradation associated with gable collapse. This approach has been applied to both numerical analyses of a Dutch URM building subjected to induced seismicity, and the use of real tectonic recordings from a monitored URM school in Italy. In both cases, induced and tectonic earthquake signals are evaluated at attic floor and gable top (ridge beam) level, and the corresponding results are reported and discussed in Section 3. Based on these outcomes, the final protocol for the experimental campaign is defined (Section 4), followed by the conclusions of this work (Section 5).

2. Methodology

2.1. Derivation of input motions for the induced earthquake scenario

2.1.1. Building typology adopted for the numerical simulations

Within the ERIES-SUPREME project, one of the reference building stocks is that of the Groningen province (NL), an area affected by human-induced earthquakes resulting from gas extraction activities. The majority of the existing building stock in this region consists of low-rise URM structures, not designed to withstand seismic loads [76], which commonly feature gables supporting timber roofs. These buildings are therefore relevant for deriving input motions representative of induced seismicity, characterised by low intensity and short significant duration, in support of the ERIES-SUPREME experimental campaign. An idealized terraced house, typical of the Groningen region, is selected as reference

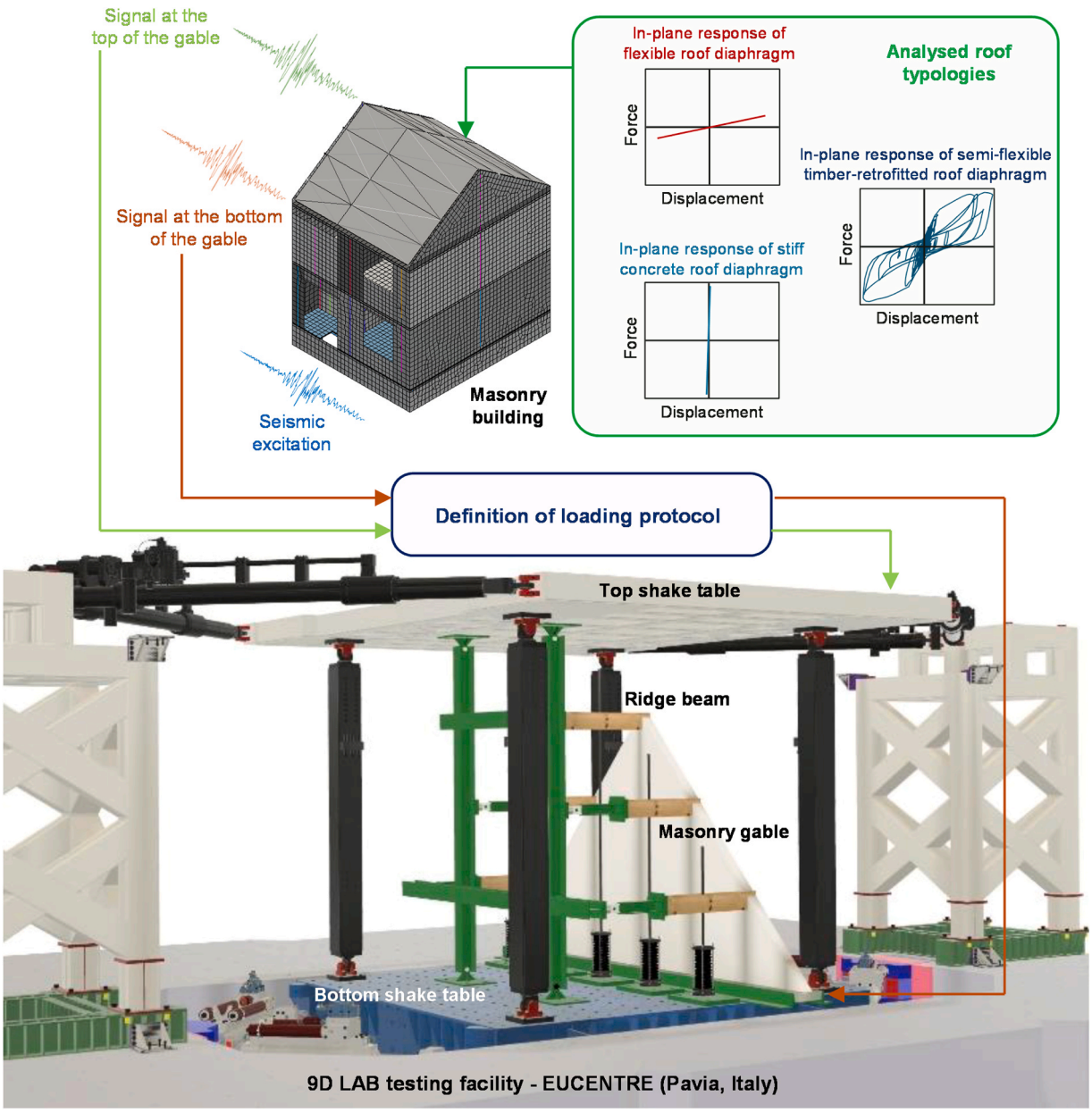

Fig. 1. Methodology for defining the loading protocol for induced input accelerograms employed in the experimental campaign of the ERIES-SUPREME project [64], starting from numerical time-history analyses on a reference URM building with three different roof typologies.

building typology for predicting the seismic motion acting at base and top of masonry gables (Fig. 2a). This selection is based on a previously investigated structure [77], with its main characteristics and modelling assumptions maintained for the present study. The selected building has in-plan dimensions of 7.3 × 6.1 m, and an overall height of 8.2 m; each storey and the gables have height of approximately 2.7 m. The building relies on URM cavity walls: the inner leaf and internal walls are made of 100-mm-thick calcium-silicate (CS) bricks, the outer leaf is made of 100-mm-thick clay brick masonry, and steel ties provide the connection between the two leaves. The terraced house consists of two floors and an attic level. The ground floor is made of prefabricated arched concrete elements, the first and second (attic) floors are made of cast-in-situ reinforced concrete (RC) slabs, while the roof is made of timber purlins and trusses with concrete roof tiles [77]. Overall, the selected house features a sufficiently stiff and resistant masonry structure with rigid floors up to the attic level and a flexible roof with slender gables. This makes this building a relevant case for investigating the seismic vulnerability of the gables and their interaction with the roof structure.

A variety of numerical modelling strategies (including but not limited to [78–89]) can be used to simulate the seismic response of URM buildings. In this study, the numerical model of the building is created in the finite element software DIANA FEA version 10.6 [90]. The masonry walls are simulated using shell elements featuring the *Engineering Masonry Model* (EMM) [91,92], a total-strain based continuum model that accounts for tensile, shear and compression failure of the masonry. All internal 100-mm-thick CS walls are explicitly modelled to include their stiffness and strength to the whole building response. However, while the loadbearing internal walls, running transversely in the middle of the building unit, are fully connected to both bottom and top floor and to the longitudinal external façades with openings (Fig. 2a), the non-loadbearing internal walls are disconnected from the floor above so that no force may be transferred. In addition, the lateral wall-to-wall connections with the transverse external façades (without openings, Fig. 2a) are modelled with strips of weak elements, having mechanical

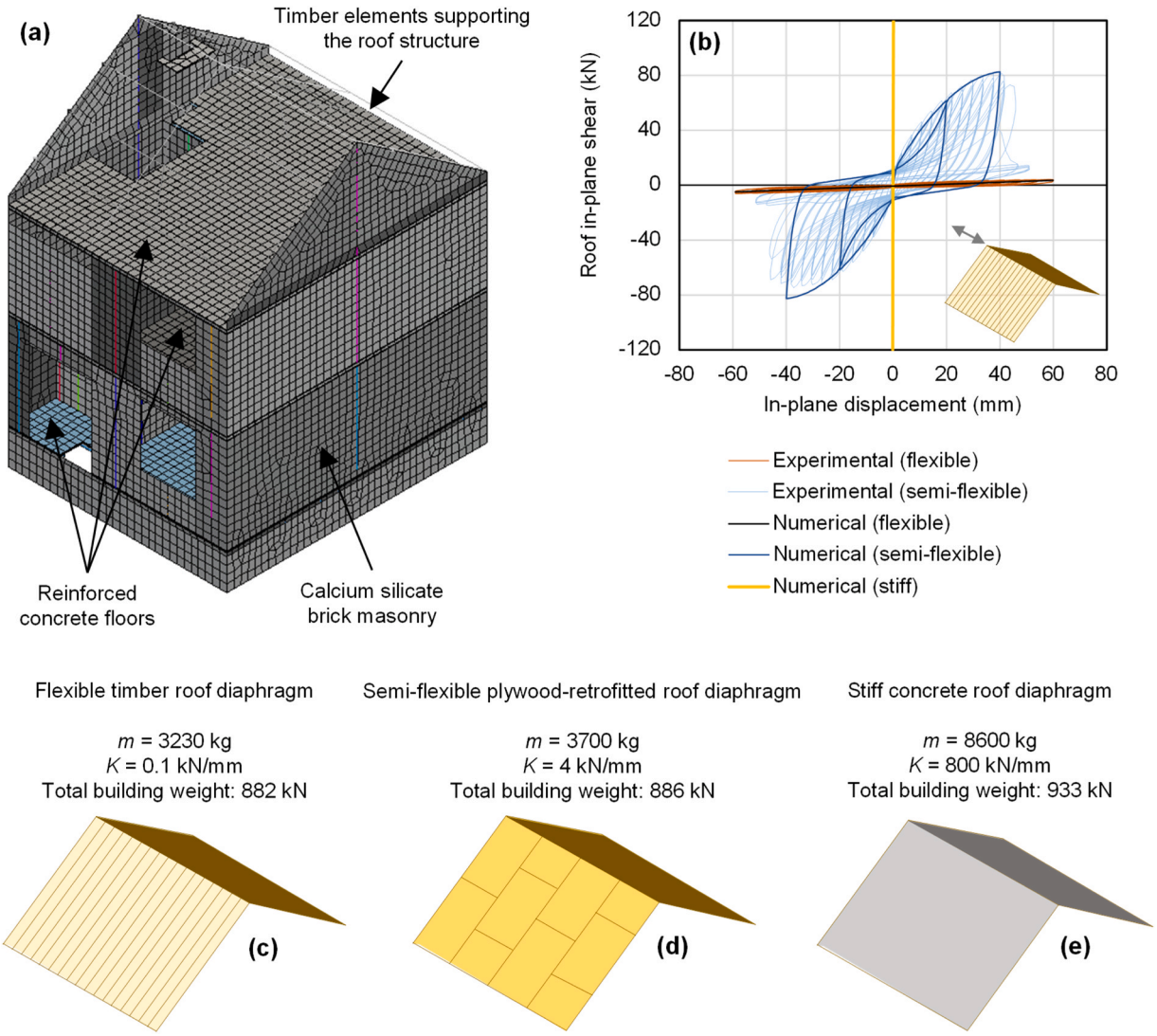

Fig. 2. Model of the reference building in DIANA FEA (a) and analysed roof configurations as implemented in the numerical model in comparison to available experimental tests (b): flexible (existing) timber roof structure (c); semi-flexible roof retrofitted with plywood panels (d); stiff (retrofitted) concrete roof (e). The symbols m and K denote the mass and secant in-plane stiffness of the roof diaphragms at 10 mm distortion, respectively.

properties reduced by 30 %, and simulating vertical mortar joints [77]. Given the negligible shear stiffness of the wall ties [93,94], they are assumed to transfer only axial loads. For this reason, the cavity-wall system is simulated by explicitly modelling the loadbearing inner leaf, while the outer leaf is considered as dynamic mass, having a specific weight of 14 kN/m^3 [77], acting in the wall out-of-plane direction and contributing only to the inertial forces in nonlinear time-history analyses [90]. The main properties of the external and internal masonry walls adopted for the numerical model are reported in Table 1. For masonry elements, a mesh size of 200 mm is adopted, in agreement with previously conducted analyses on similar URM buildings [95,96].

The concrete floors are simulated via non-linear shell elements, using the *Total Rotating Strain Crack Model* for the concrete and the *Von Mises Plasticity Model* for the steel reinforcement [77]. A Young's modulus of 27000 MPa, and uniaxial tensile and compressive strength of 1.57 MPa and 20 MPa, respectively, are assumed for concrete, while a Young's modulus of 200000 MPa and yield strength of 400 MPa are adopted for the rebars [77].

The timber purlins, struts, ties and the ridge beam supporting the roof structure, are modelled by means of linear elastic isotropic beam elements with a Young's modulus of 9000 MPa [77]. The connections between the gables and the purlins or ridge beams are simulated through point interface elements using a Coulomb friction material model with cohesion of 0.02 MPa and friction coefficient of 0.6, to capture the potential sliding of the beams in the pocket connections [77].

All structural element geometries and properties are kept identical

Table 1
Reference properties for the shell elements representing masonry walls in the numerical model [77].

Property	Value
Young's modulus perpendicular to bed joint E_y [MPa]	4000
Young's modulus parallel to bed joint E_x [MPa]	2667
Shear modulus G [MPa]	1650
Density ρ [kg/m^3]	1850
Bed-joint (tensile) strength f_y [MPa]	0.15
Minimum head-joint strength $f_{x,min}$ [MPa]	0.30
Fracture energy in tension $G_{f,I}$ [N/m]	10.0
Angle between stepped diagonal crack and bed joint α [rad]	0.62
Compressive strength f_c [MPa]	7.0
Fracture energy in compression G_c [N/m]	15000
Friction coefficient	0.60
Cohesion c [MPa]	0.25
Fracture energy in shear G_s [N/m]	100

for all models presented in this study, with the only key variable being the roof structure. Indeed, three roof configurations are accounted for in the reference full-scale experimental shake-table tests on masonry gables. Therefore, the analysis first focuses on the as-built state of a terraced house with a flexible timber roof, whose behaviour can be approximated as linear elastic (Fig. 2b, c). A second case involving a roof retrofitted with timber-based techniques having a semi-flexible, nonlinear, dissipative behaviour is considered (Fig. 2b, d). Finally, a stiff concrete roof structure is also accounted for (Fig. 2b, e).

In the numerical model representing the existing terraced house with flexible roof, the properties of the timber planks are derived based on previous experimental and analytical studies on as-built wooden roof structures typical for the Groningen area [56]. The roof planks are modelled with linear elastic orthotropic shell elements, whose properties are reported in Table 2 and are consistent with the limited secant stiffness observed during an in-plane cyclic test on a replicated timber roof from the Groningen region (Fig. 2b, c). In this case, nonlinearities are not taken into account because of the very limited energy dissipation observed in related experiments (Fig. 2b) [56].

The timber-based retrofitted roof (Fig. 2b, d) allows the study of a configuration with intermediate stiffness between the as-built and the stiff case, and its effect on the out-of-plane response and related accelerations of the gables. The considered timber-based retrofit consists of an overlay of plywood panels fastened to the existing planks. This solution greatly improves the in-plane strength and stiffness of diaphragms, also providing beneficial energy dissipation [45,50,52–58,97]. To accurately simulate the in-plane response of such structure, a macro-element strategy was adopted, whose analytical and numerical background is described in detail in [97,98]. The mesh of macro-elements consists of quadrilaterals made up of rigid truss elements, hinged each other and surrounding two diagonal truss elements, in which the nonlinear response of the roof is implemented by means of a previously developed user-supplied subroutine running in DIANA FEA [98]. The macro-elements are overlaid onto the shell elements representing the existing timber planks described above, and are calibrated according to the approach reported in [98], with reference to an experimentally tested plywood-strengthened roof sample [56]. The resulting nonlinear cyclic in-plane response of this roof configuration up to a deflection of 40 mm is shown in Fig. 2b, and is consistent with the related experimental results, in terms of transferred in-plane shear and pinching behaviour [56].

Finally, in the case of the stiff roof configuration (Fig. 2b, e), a concrete slab cast fully collaborating with the existing roof structure is assumed, simulating a retrofitting solution widely adopted in the past. The properties of the linear elastic shell elements simulating the roof are then assumed as those of reinforced concrete (Young's modulus $E = 30000$ MPa, shear modulus $G = 13000$ MPa with Poisson's ratio $\upsilon = 0.15$, density of 2500 kg/m^3).

2.1.2. Conducted numerical analyses

For all the developed models, modal analyses and incremental nonlinear dynamic (time-history) analyses are performed. The modal analyses allow to compare the flexible, semi-stiff, and stiff configurations in terms of eigenfrequencies and mode shapes, with specific reference to the gable level (Section 3.1). The time-history analyses are conducted based on an accelerogram representative of induced seismicity, scaled up to an intensity that has proved to be significantly severe for the selected building typology [77]. The accelerogram features a Peak Ground Acceleration (*PGA*) of 0.14 g, corresponding to the design acceleration specified for the original building location, as indicated in the NPR 9998 web tool [75], an interactive digital platform designed to assist engineers and stakeholders in applying the Dutch seismic guidelines NPR 9998 [74]. The input signal is applied to the models at the bottom of the building, along the direction perpendicular to the plane of the gable, so as to reproduce the same loading conditions of the ERIES-SUPREME experimental campaign.

The dynamic simulations for deriving the induced seismicity records at the top and bottom of the gables, are performed at various intensity levels, up to a *PGA* of 0.27 g, with the structure exhibiting different levels of damage at each intensity. The records selected for testing, shown in Sections 3.1 and 4, are ultimately taken with reference to minor to moderate structural damage (DS2-DS3) for the building, in order to avoid unrealistically high amplifications, and are then scaled according to the requirements of the testing sequence (Section 4). The adopted induced accelerogram combines the original design motion [75], already provided under conservative assumptions in terms of amplitude, duration, and hazard models, with a large scaling factor. This scaling was primarily selected to induce sufficient damage and OOP displacements in the gable walls for all three configurations, thereby enabling the characterisation of the roof's filtering action beyond the elastic range in the modelled URM house, which ultimately allows to appreciate the desired damage levels during the shake-table tests. Additionally, the intensity of the scaled motion is comparable with the highest and most conservative design-level hazard defined for the Groningen province in [75]. However, it is important to note that the amplified motion is not meant to reflect the actual seismic hazard in the area, where the largest recorded *PGA* to date was equal to 0.11 g, observed during the ML 3.4 Zeerijp earthquake on January 8th, 2018 [99]. Besides, the complete gas field closure, become definitive in 2024, is expected to further reduce the seismic hazard in the area. For these reasons, stronger induced earthquake signals are not considered, and input motions derived from tectonic earthquakes are adopted to test the gables up to extensive structural damage and failure, covering higher seismic intensities and longer significant durations (Sections 2.2 and 4).

Table 2
Reference properties for the shell elements representing timber roof sheathing in the numerical model.

Property	Value
Young's modulus E_x [MPa]	10000
Young's modulus E_y [MPa]	10000
Young's modulus E_z [MPa]	10000
Density [kg/m^3]	380
Poisson's ratio υ [-]	0.15
In-plane shear modulus G_{xy} [MPa]	2.0
Shear modulus G_{yz} [MPa]	625
Shear modulus G_{xz} [MPa]	625

2.2. Derivation of input motions for the tectonic earthquake scenario

For the definition of the tectonic input motions, a real-case scenario has been selected, since actual earthquake recordings are available. In particular, a monitored two-storey masonry building used as an elementary school, located in Visso (Province of Macerata, Italy) is considered [69,70,100,101]. This structure features regular undressed stone masonry walls, with a thickness of 66–87 cm, and consisting of approximately 30 × 15 cm double wythe blocks, with header stones connecting the two wythes [100]. Rigid diaphragms, composed of one-way concrete slabs with joists and hollow clay elements, are present at ground and first floor, while a more flexible diaphragm made of steel joists and hollow clay elements is located at attic level.

This building is part of the network of the Seismic Observatory of Structures (OSS), coordinated by the Italian Department of Civil Protection [69]. This network comprises a series of buildings and bridges across Italy equipped with a monitoring system. As part of the monitoring system, several accelerometers are placed within the building (Fig. 3): among them, one at ground floor (NF in Fig. 3c) and one at the attic floor level (A8 in Fig. 3c) have been selected, with the latter precisely corresponding to the needed input for the bottom shake table. The recordings of these accelerometers during the 2016 earthquakes that struck Central Italy, represent a reliable tectonic seismic excitation at the gable level for the desired extensive structural damage state (DS4),

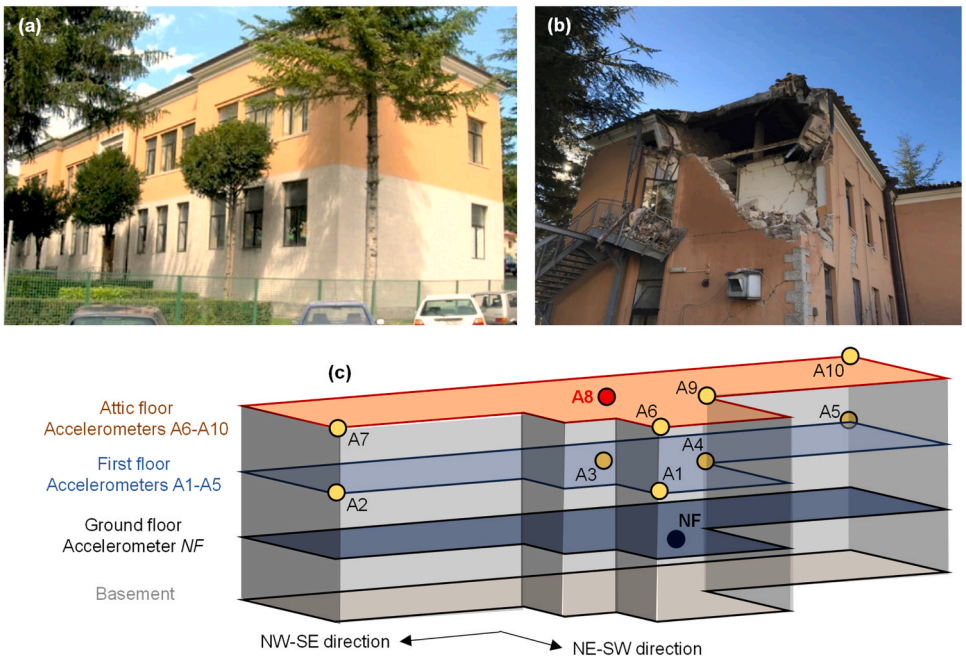

Fig. 3. Views of the monitored URM building selected for the definition of the tectonic input motions before (a) and after (b) the 2016 Central Italy earthquakes [100],[101]; schematic 3D representation of the building with overview of available and selected (NF and A8) accelerometers (c).

considering also the partial collapse of the building during this earthquake sequence (see Fig. 3b and Section 3.2).

Based on the recorded signal at the attic level of the selected URM structure, the influence of the roof stiffness in the response of the gables is then studied by employing an elastic single-degree-of-freedom (SDOF) system to simulate the gable-roof interaction and determine the acceleration at the roof ridge (top of the gable), as further discussed in Section 3.2.

3. Results

3.1. Numerical analyses of the reference Dutch terraced house subjected to induced seismicity

The three roof configurations in the reference URM terraced house are first compared in terms of results from modal analysis: the vibration periods in the OOP direction of the gables and mode shapes obtained for them are illustrated in Fig. 4. When considering the as-built configuration (Fig. 4a), a local OOP mechanism involving the overturning of the gables is observed, due to the flexible roof structure. Although this local mode involves participating mass factor of 10 % of the total mass, it is relevant as it highlights the mechanism at the level of the roof-gable system, a typical failure mode observed in case of a flexible roof diaphragm. In contrast, both the configurations with semi-flexible and stiff roof exhibit a stiffer response with lower periods, and mode shapes uniformly engaging the whole building, as expected (Fig. 4b, c); this is also reflected in the larger participating mass factor associated with these modes (67 % and 69 % of the total mass, respectively). Interestingly, the periods of the configurations with semi-flexible and stiff roof diaphragms are practically identical. This can be attributed to the fact that the in-plane stiffness of the diaphragms is in both cases very large relatively to the OOP stiffness of the gables, leading to the observed global mode shapes and large participating masses, as opposed to the flexible roof diaphragm configuration.

The outcomes from the nonlinear time-history analyses are presented in the following in terms of accelerations (Fig. 5) and displacements (Fig. 6) recorded at the bottom and at the top of the gable. Specifically, these control nodes are located at a point on the attic just below the centre of the gable wall, and at the extremity of the ridge beam above the top of the gable, in the case of a timber roof, or at a point of the concrete

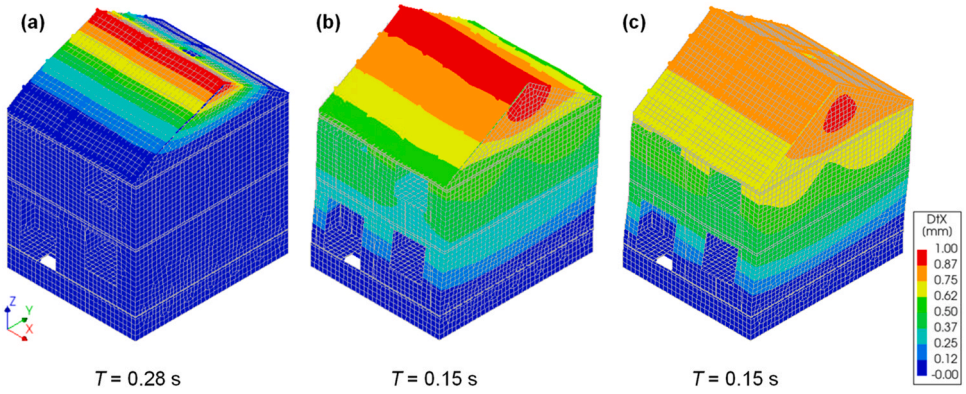

Fig. 4. Modal analysis results: vibration modes and 3D displacement distribution rendering in the OOP direction of the gables within the building, with flexible (a), semi-flexible (b), and stiff (c) roof.

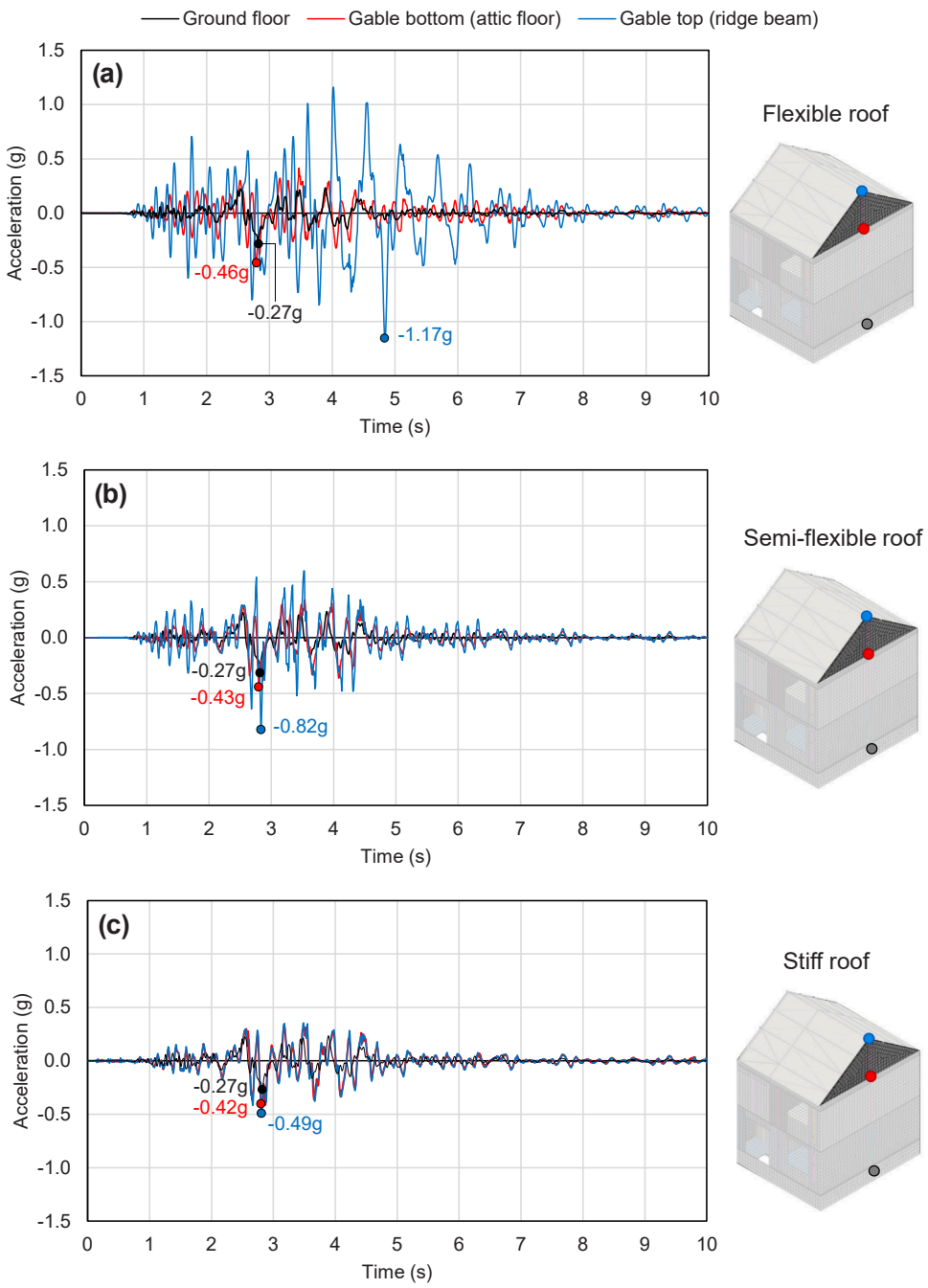

Fig. 5. Accelerations recorded at the bottom and top of the gable for the design-level induced earthquake signal imposed at the base of the building (*PGA* = 0.27 g): flexible (a), semi-flexible (b), and stiff (c) roof configuration. Peak acceleration values at each locations are highlighted.

slab next to the top of the gable, in the case of a concrete roof, indicated in Fig. 5 as a red or blue dot, respectively. Additionally, the crack pattern of the gable walls is shown (Fig. 7). All these results refer to the same input accelerogram for the building imposed at its base, scaled at a *PGA* of 0.27 g.

The acceleration time histories recorded for the bottom and top of the gables are shown in Fig. 5. When examining the signals at the bottom of the gable (attic floor), the peaks and corresponding frequencies are very similar for all the three configurations for the examined building: at the attic level an amplification of the acceleration of approximately 1.5 times the input ground motion is observed, corresponding to values of 0.42–0.46 g (Fig. 5). The effect of roof stiffness becomes apparent when comparing the signals simulated at the top of the gables. As expected, the accelerations progressively decrease as the stiffness of the roof structure increases. Furthermore, in the case of the flexible roof (Fig. 5a), the signal not only shows an acceleration amplification of up to 2.8 times compared to the accelerogram at the attic level, but is also out of phase. Compared to the other roof configurations, this induces an earlier damage and an OOP displacement of more than half of the gable thickness, which could be associated with an OOP failure of the gable. The presence of a semi-flexible roof (Fig. 5b), which can also dissipate part of the energy imparted by the earthquake, results not only in a reduction of the acceleration amplification with respect to the attic level (up to 1.7 times), but also in an in-phase response. Finally, with a stiff roof (Fig. 5c), the amplification effect at the top of the gable is negligible, as expected.

Fig. 6 shows the relative displacement between the roof top and the attic recorded during the performed time-history analyses. This

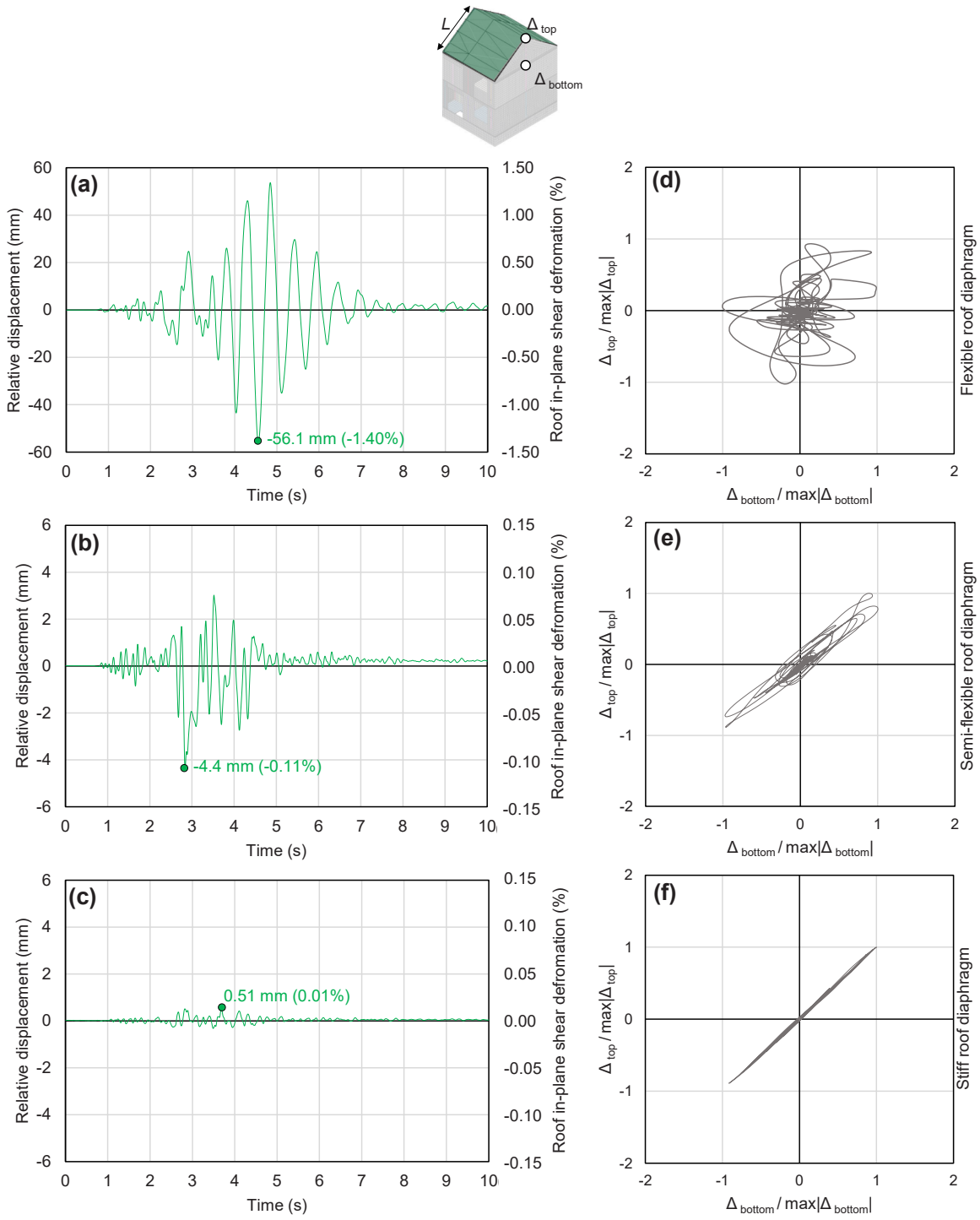

Fig. 6. Relative displacements ($\Delta_{top} - \Delta_{bottom}$) between top and bottom of the gable and corresponding in-plane shear deformations (relative displacements over the span L of one pitch) of the flexible (a), semi-flexible (b), and stiff (c) roof configuration recorded for the design-level induced earthquake signal imposed at the base of the building ($PGA = 0.27$ g); corresponding Lissajous diagrams [36] highlighting phase shift for flexible roof diaphragm (d), and progressively in-phase motion for semi-flexible (e) and stiff (f) roof diaphragms.

corresponds to the in-plane deformation of the roof structure, and relates to the hysteretic behaviour of each of the three considered configurations. These graphs confirm the previous outcomes analysed in terms of accelerations, and are consistent with the roof stiffness of each model. The same input ground motions generate large in-plane displacements in the flexible roof (Fig. 6a), which could potentially lead to the OOP collapse of the gable. In contrast, these displacements are limited for the semi-flexible configuration (Fig. 6b), although sufficient to activate energy dissipation in the diaphragm. The stiff roof, as expected, shows negligible in-plane displacements (Fig. 6c). Furthermore, the previously observed transition from a phase shift in the seismic motion of the flexible roof diaphragm to a more in-phase response of the semi-flexible and stiff roof configuration, is also confirmed by constructing the Lissajous diagrams [36] corresponding to the recorded displacement time-histories at the top (Δ_{top}) and bottom (Δ_{bottom}) of the gable (Fig. 6d-f). This representation is useful for highlighting phase

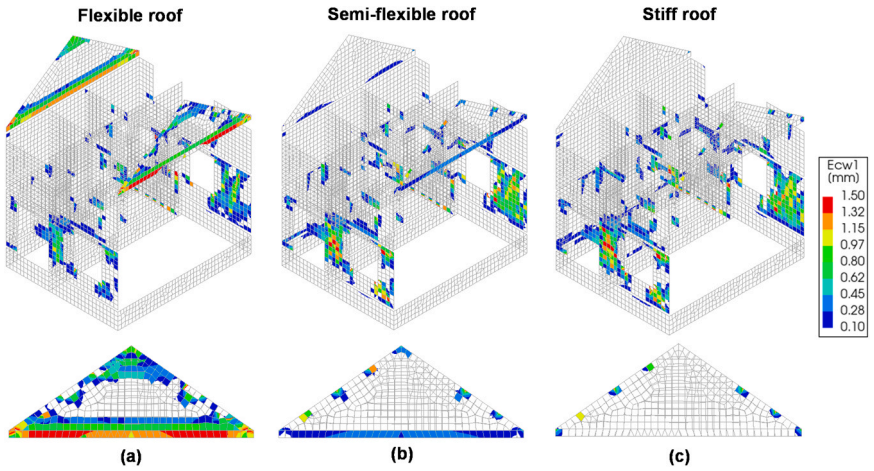

Fig. 7. Crack pattern for the whole building and for the gables developed during the induced earthquake signal imposed at the base of the house (*PGA* = 0.27 g). In the contour plot legend, the upper limit for the principal crack width is set at 1.5 mm to enhance and compare the damage; the actual recorded maximum width is 7.29 mm for the flexible roof case (a), 6.24 mm for the semi-flexible roof case (b), 6.51 mm for the stiff roof case (c). Floors and right out-of-plane walls below the attic level are hidden to better show all in-plane walls and the gables.

shift in seismic signals and has previously been adopted to describe the OOP response of URM walls subjected to relative support motions [36]. The diagrams are constructed by plotting together Δ_{top} and Δ_{bottom}, normalizing them by dividing by their absolute maximum values $\max|\Delta_{top}|$ and $\max|\Delta_{bottom}|$, respectively (Fig. 6d-f).

The crack patterns of the whole building and close-ups of the gables are shown in Fig. 7. The presence of a flexible roof diaphragm (Fig. 7a) corresponds to extensive OOP cracks and damage especially at the base of the gables, along with limited in-plane damage to the piers at the lower building storeys. In both the semi-flexible (Fig. 7b) and stiff (Fig. 7c) roof, the building exhibits a more favourable global box-type response, with a significantly lighter crack propagation in the gables and more spread in-plane damage in the piers. A slightly more pronounced in-plane damage on the masonry piers is observed for the stiff roof configuration, due to the larger mass and the absence of hysteretic energy dissipation activated in the diaphragm, as opposed to the semi-flexible configuration.

3.2. *Tectonic seismic signals from the referenced monitored building in Italy*

The selected recordings of the 2016 Central Italy earthquake from the monitored school in Visso (Section 2.2) are reported in Fig. 8a for the ground and attic floor. The selected signal is a strong motion recorded in Ussita (Macerata, Italy), with the epicenter located 4 km away, corresponding to a magnitude 5.9 event that occurred on October 26, 2016, at 19:18:04 UTC. The chosen direction is NW-SE (Fig. 3c), with a *PGA* of 0.365 g. This direction has been selected because the seismic signal features a smooth response spectrum, in line with that related to the induced earthquake signal, and is associated with a displacement demand in continuity with the induced earthquake scenario. It is interesting to notice that, also for this real-case URM building, an acceleration amplification of approximately 1.5 times is observed at the attic level compared to the ground. The recorded signal at the attic floor, representative of tectonic seismicity, is directly imposed at the bottom of the gables in the reference experimental campaign (Section 4).

Starting from the signal recorded at the attic level of the monitored building, the influence of the roof stiffness on the response along the height of the gable is accounted for, considering the results obtained by the performed numerical analyses for the induced seismicity scenario (Section 3.1). Specifically, in the stiff roof scenario, the same signal recorded at the attic level is assumed for the top of the gable, due to the negligible difference observed between the two. For the semi-flexible roof configuration, the signal at the top of the gable is assumed as an amplification of the motion at the attic floor (bottom of the gable) by a factor of approximatively 1.7 (Section 3.1), neglecting any phase shifting as suggested by numerical analyses on this roof configuration. Finally, for the flexible roof scenario, an elastic single-degree-of-

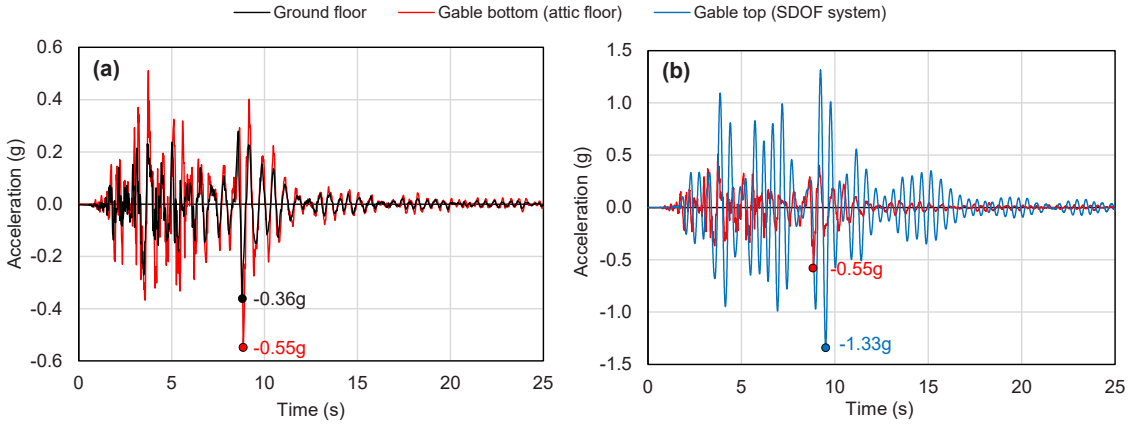

Fig. 8. Signals recorded during the 2016 Central Italy earthquake in the reference URM school at ground and attic floor (a); derivation of the signal at the top of the gable for the flexible roof scenario using SDOF system (b). Peak acceleration values at each locations are highlighted.

freedom (SDOF) system is employed to simulate the gable-roof interaction (Section 2.2) and determine the acceleration at the roof ridge (i.e., top of the gable). Thus, the signal at attic level is applied to the SDOF system, featuring a period $T_{SDOF} = 0.5$ s and a damping ratio $\zeta_{SDOF} = 5$ %, both representative of the in-plane response of flexible timber roofs [56], resulting in a significant acceleration amplification at the top of the gable (ridge beam), and thus a large displacement demand typical of an as-built roof structure with gables (Fig. 8b). Consistently with the induced seismicity scenario, an out-of-phase response and a amplification factor of approximately 2.6 between bottom and top of the gable, are obtained.

4. Definition of the testing protocol for the ERIES-SUPREME experimental campaign

The acceleration signals presented in Sections 3.1–3.2 serve as basis to define the testing protocol for the shake-table tests on the full-scale masonry gables. The following key results have been considered in the design of this protocol. First, in both induced and tectonic earthquake scenarios, the structure of the building amplifies the bottom seismic excitation by a factor 1.5 from foundations up to the attic level. This demonstrates that even with no amplification at the roof, the building itself significantly filters the motion applied at the ground level, as confirmed by both the actual recordings of tectonic earthquakes and the numerical analyses under induced seismic events. Second, in the case of the flexible roof, the ridge beam supported at top of the gables experiences an acceleration amplified by up to 2.8 times compared to the attic floor. Notably, the two signals are out of phase, which contributes to early damage and potential failure of the gables. The recorded amplification appears to be consistent with previous results from experimental shake-table tests on URM buildings with flexible roofs, ranging from a value of 2.3 [40] to 2.9 [44] at collapse-prevention limit state (DS4). For the semi-flexible roof configuration, while the ridge beam (corresponding to the top of the gable) still experiences an acceleration amplified by up to 1.7 times compared to the base of the gable, the two signals remain in phase. Finally, with the stiff roof configuration, the accelerations at the top and bottom of the gable are almost identical, indicating no amplification as expected.

The adopted protocol considers the type and intensity of the applied signals, as well as the technical capabilities and general characteristics of the 9D LAB system. As shown previously in Fig. 1, the top shake table is positioned at a greater height (h_{top}) than that of the ridge beam (h_{ridge}). This difference is accounted for in the testing protocol by defining the corresponding input acceleration for the top shake table as:

$$a_{top} = (a_{ridge} - a_{attic}) \cdot h_{top} / h_{ridge} + a_{attic} \quad (1)$$

In Eq. 1, a_{ridge} and a_{attic} are the accelerations at top and bottom of the gables recorded in the numerical analyses, while the ratio h_{top} / h_{ridge} is quantified based on the known geometry of test setup and gable:

$$h_{top} / h_{ridge} = 3750 \text{ mm} / 2900 \text{ mm} \approx 1.3 \quad (2)$$

This adjustment is applied for both induced earthquake signals, used as input motions up to $PGA \leq 0.30$ g, and tectonic earthquake signals, used as input motions for $PGA > 0.30$ g.

Starting from either the motion recorded via the numerical simulations for an induced earthquake or the recorded tectonic motion to be applied for all roof configurations to the bottom shake table (simulating the attic level of a URM building) of the 9D LAB, the input signal for the top shake table is defined as follows:

- For the stiff roof scenario, the same signal applied to bottom shake table is equally applied also to the top one, given the negligible difference between the responses at the bottom and top of the gable.
- For the semi-flexible roof scenario, the input motion at the top shake table is defined as an amplification of the signal at the bottom by a factor of 2.0, applicable to both induced and tectonic motions. This factor incorporates the roof stiffness amplification factor of approximately 1.7 (Section 3.1) and the geometrical characteristics of the test setup (as detailed in Eq. 1). This assumption is considered valid due to the negligible, and nearly experimentally unreproducible, phase shift observed between the base and the top of the gable in the numerical analysis (Fig. 6e). Furthermore, considering the main intention of the experiments to be numerical benchmarks, for a more robust calibration or validation of numerical models developed on the basis of the test results, it is convenient to separately asses the effects of the signal amplification, addressed in this scenario, and those of the amplification combined with phase shift (flexible roof scenario). By considering a 2 × amplification of the signal applied at the bottom of the gable, larger relative displacements are obtained between the top and bottom of the gable compared to the numerical results presented in Fig. 6b (see Table 3).
- For the flexible roof scenario, a distinction is made between the induced and the tectonic earthquake scenarios. In the former case, the accelerations recorded via the numerical simulations at the attic and the ridge beam (Section 3.1) are used, and the final motion is obtained by applying Eq. 1. In the latter scenario, the recorded attic floor signal is considered and filtered through the adopted SDOF system (Section 3.2), with Eq. 1 also applied to finally derive the input motion for the top shake table.

The induced and tectonic input signals at the bottom (attic floor) and top (ridge beam) of the gable are shown and compared in Fig. 9, along with the corresponding response spectra to highlight their frequency content. Table 3 complements this information by summarising typical strong motion characteristics for the selected motions, differentiating between induced and tectonic seismicity as well as among the ground floor (i.e., the original signal at the base of the building), the attic floor (i.e., bottom of the gable) and the roof ridge (i.e., top of the gable). These strong motion characteristics include peak ground acceleration (*PGA*), peak attic floor acceleration (*PFA*), peak ridge acceleration (*PRA*), average spectral acceleration ($S_{a,avg}$) between 0.02 s and 0.67 s (i.e., between the uncracked and cracked period of the gable [64]), cumulative absolute velocity (*CAV*), Arias Intensity (I_A), Housner Intensity (I_H) between 0.1 s and 2.5 s, 5 %-95 % significant duration ($D_{5–95}$), period corresponding to the maximum spectral acceleration (T_d), and the maximum absolute value of the relative displacement between the ridge and the attic floor (Δ_{max}).

The final testing protocol for the ERIES-SUPREME experimental campaign is then established by progressively scaling both induced and tectonic earthquake signals. The induced-motion tests begin with a scaling factor of 0.10, followed by increments of 0.10 up to 0.50, after which the scaling factors increase to 0.75 and 1.00. To ensure some continuity between the two input scenarios, tectonic motion tests start with a scaling factor of 0.50 and increase by increments of 0.25 until reaching 2.50. Additional tests beyond a scaling factor of 2.50 are conducted with increments of 0.50.

5. Conclusions

This work has discussed the selection of the input motions in support of the out-of-plane dynamic shake-table testing of masonry gables at the 9D LAB facility at EUCENTRE (Pavia, Italy). The goal is to characterise their out-of-plane (OOP) response as a function of the roof stiffness within the ERIES-SUPREME research project, considering both induced and tectonic earthquake scenarios. To investigate the former case, advanced numerical analyses have been performed on a reference masonry building typical for the province of Groningen (NL), which is subjected to induced seismicity. The main seismic vulnerability of the selected building is related to the presence of a flexible roof structure and slender masonry gables, prone to local OOP collapse. The building has been investigated in the existing (as-built) condition with a flexible

Table 3
Summary of main strong motion characteristics associated with the selected earthquake signals.

Strong motion characteristics	Design-level induced seismicity motions				Recorded tectonic seismicity motions			
	Ground floor	Attic floor*	Ridge		Ground floor	Attic floor*	Ridge	
	All scenarios	All scenarios	Semi-flexible	Flexible	All scenarios	All scenarios	Semi-flexible	Flexible
PGA [g]	0.27	-	-	-	0.36	-	-	-
PFA [g]	-	0.42	-	-	-	0.55	-	-
PRA [g]	-	-	0.75	1.19	-	-	0.96	1.33
$S_{a,avg}$ [g]	0.53	0.86	1.53	2.67	0.67	1.14	2.02	2.78
CAV [m/s]	2.97	5.35	9.48	17.6	8.88	14.3	25.3	47.2
I_A [m/s]	0.44	1.32	4.15	12.0	1.54	3.87	12.2	37.4
I_H [m]	0.81	0.95	1.69	2.24	1.01	1.41	2.50	3.44
D_{5-95} [s]	2.70	2.92	2.92	4.23	7.75	7.55	7.55	10.5
T_d [s]	0.48	0.22	0.22	0.50	0.68	0.66	0.66	0.50
Δ_{max} [mm]	-	-	25.4	56.8	-	-	42.5	82.2

* The same motion is also applied at the ridge in the case of the stiff roof scenario.

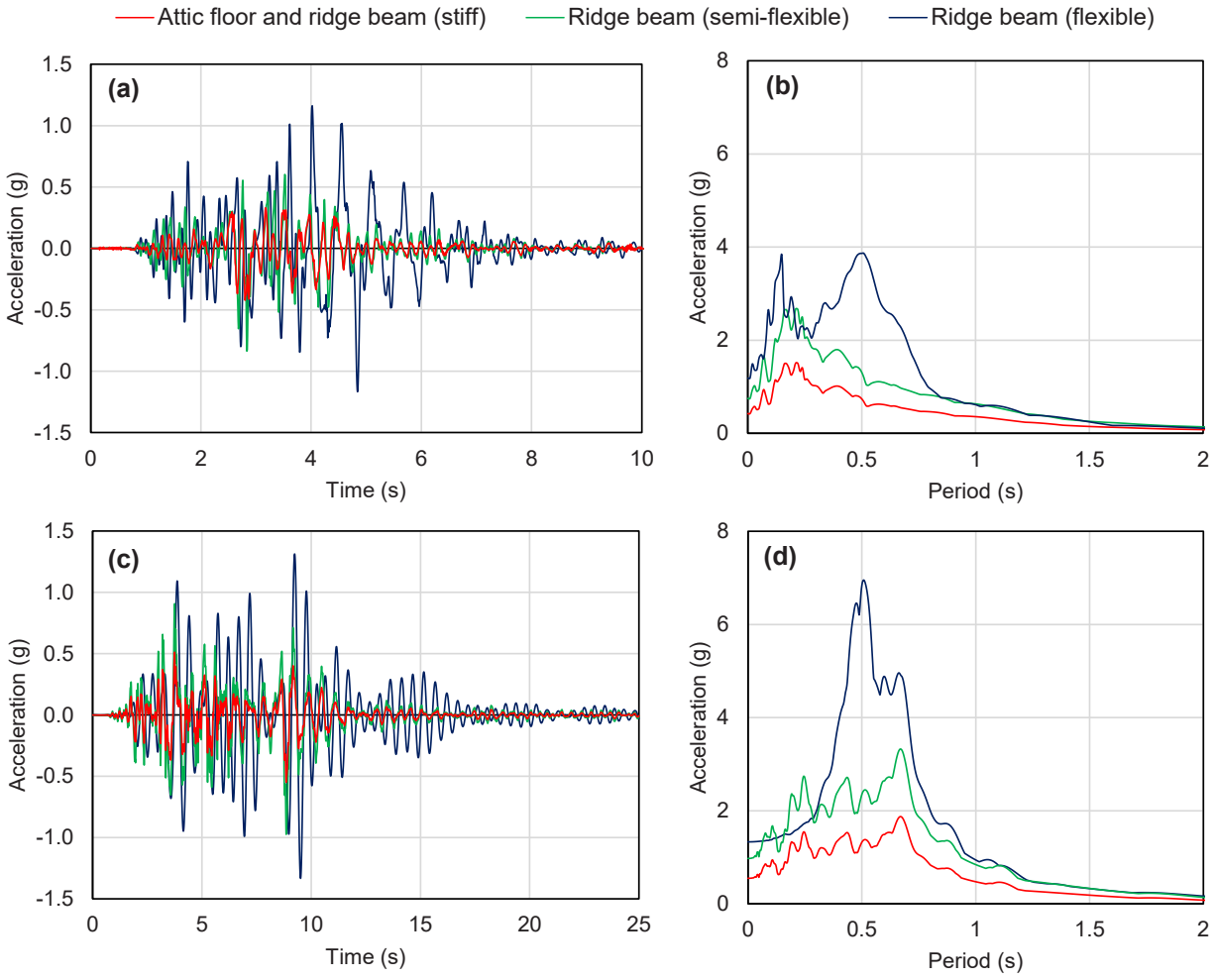

Fig. 9. Accelerograms at the bottom (attic floor) and top of the gable (ridge beam) for the three roof scenarios (stiff, semi-flexible, and flexible): acceleration time-histories (a) and corresponding response spectra (b) for design-level induced seismicity motion; acceleration time-histories (c) and corresponding response spectra (d) for recorded tectonic seismicity motions.

timber roof, as well as in two retrofitted conditions: one with a stiff concrete roof, and another with a semi-flexible roof strengthened with a timber-based intervention, representing an intermediate situation. To investigate the tectonic earthquake scenario, a monitored masonry building in Italy has been selected, from which the recordings of the 2016 Central Italy earthquake at ground and attic floor level are available. At attic level, the recorded amplification of the base excitation caused by the building was 1.5 times, the same resulting from the numerical analyses related to the induced earthquake scenario. The gable-roof interaction for the flexible roof scenario simulated with the adopted elastic SDOF system was also very similar, with an out-of-phase response amplified by up to 2.8 times. Consistently with the numerical outcomes, for the semi-flexible roof scenario, the signal at ridge beam consisted of that at attic level amplified by 1.7 times, while for the stiff roof case the

same signal was considered.

Based on these findings and assumptions, the testing protocol has been defined by taking into account the characteristics of the 9D LAB facility, and combining the effects of both induced and tectonic seismic signals, which allow to reproduce moderate and extensive structural damage, respectively. The selected input motions feature smooth response spectra, and ensure continuity in the spectral accelerations and displacement demands between the two different earthquake scenarios throughout the testing protocol. The adopted signals serve as the input motions for the bottom and top shake tables in the 9D LAB, allowing for the investigation of the gable dynamic response. For the induced earthquake scenario, these motions result in in maximum relative displacements between gable top and bottom of 57 mm and 25 mm for the flexible and semi-flexible configuration, respectively; the stiff configuration show no relative displacement. For the tectonic earthquake scenario, these relative displacements are equal to 82 mm and 43 mm for the flexible and semi-flexible configuration, respectively; also in this case, the stiff configuration show no relative displacement. Thus, this protocol allows to account for different roof stiffnesses and ground motion typologies, forming the basis for a comprehensive investigation on how these factors influence the dynamic out-of-plane response of masonry gables. The results of the ERIES-SUPREME experimental campaign are planned to be presented in an upcoming dedicated publication.

CRediT authorship contribution statement

Francesco Messali: Writing – review & editing, Supervision, Project administration, Methodology, Funding acquisition. **Michele Mirra:** Writing – original draft, Visualization, Methodology, Investigation, Formal analysis, Conceptualization. **Nicolò Damiani:** Writing – review & editing, Methodology, Investigation, Formal analysis, Conceptualization. **Satyadhrik Sharma:** Writing – review & editing, Supervision, Methodology, Funding acquisition, Conceptualization. **Francesco Graziotti:** Writing – review & editing, Supervision, Methodology, Investigation.

Declaration of Competing Interest

The authors declare that they have no known competing financial interests or personal relationships that could have appeared to influence the work reported in this paper.

Acknowledgements

This work is part of the transnational access project “ERIES – ERIES-SUPREME”, supported by the Engineering Research Infrastructures for European Synergies (ERIES) project (www.eries.eu), which has received funding from the European Union’s Horizon Europe Framework Programme under Grant Agreement No. 101058684. This is ERIES publication number J6. Additional funding beyond the scope of ERIES was provided by the Ministry of Economic Affairs and Climate (Ministerie van Economische Zaken, EZK) through the Netherlands Organisation for Applied Scientific Research (TNO), under contract number 3100404105 “Wandenaanpak/TU Delft”. The Authors gratefully acknowledge also Filippo Dacarro and Gerard O’Reilly for their kind support.

References

[1] Ahmadizadeh M, Shakib H. On the December 26, 2003, southeastern Iran earthquake in Bam region. Eng Struct 2004;26(8):1055–70. https://doi.org/10.1016/j.engstruct.2004.03.006.
[2] Augenti N, Parisi F. Learning from construction failures due to the 2009 L’Aquila Italy earthquake. J Perform Constr Fac 2010;24(6):536–55. https://doi.org/10.1061/(ASCE)CF.1943-5509.0000122.
[3] Binda L, Chesi C, Parisi MA. Seismic Damage to Churches: Observations from the L’Aquila, Italy, Earthquake and Considerations on a Case-Study. Adv Mat Res 2010;133–134:641–6. https://doi.org/10.4028/www.scientific.net/AMR.133-134.641.
[4] Decanini L, De Sortis A, Goretti A, Langenbach R, Mollaioli F, Rasulo A. Performance of masonry buildings during the 2002 Molise, Italy, earthquake. Earthq Spectra 2004;20(1):191–220. https://doi.org/10.1193/1.1765106.
[5] Lagomarsino S. Damage assessment of churches after L’Aquila earthquake. Bull Earthq Eng 2012;10:73–92. https://doi.org/10.1007/s10518-011-9307-x.
[6] Penna A, Calderini C, Sorrentino L, Carocci CF, Cescatti E, Sisti R, Borri A, Modena C, Prota A. Damage to churches in the 2016 central Italy earthquakes. Bull Earthq Eng 2019;17:5763–90. https://doi.org/10.1007/s10518-019-00594-4.
[7] Dizhur D, Ingham J, Griffith M, Biggs D, Schultz A. Performance of unreinforced masonry and infilled RC buildings during the 2015 Gorkha, Nepal earthquake sequence. Proc 16th Int Brick Block Mason Conf 2016:2399–407.
[8] Sharma K, Deng L, Noguez CC. Field investigation on the performance of building structures during the April 25, 2015, Gorkha earthquake in Nepal. Eng Struct 2016;121:61–74. https://doi.org/10.1016/j.engstruct.2016.04.043.
[9] Ingham J, Griffith M. Performance of unreinforced masonry buildings during the 2010 Darfield (Christchurch, NZ) earthquake. Aust J Struct Eng 2010;11(3):207–24. https://doi.org/10.1080/13287982.2010.11465067.
[10] Bayraktar A, Coşkun N, Yalçin A. Performance of masonry stone buildings during the March 25 and 28, 2004 Aşkale (Erzurum) earthquakes in Turkey. J Perform Constr Fac 2007;21(6):432–40. https://doi.org/10.1061/(ASCE)0887-3828(2007)21:6(432).
[11] Calayır Y, Sayın E, Yön B. Performance of structures in the rural area during the March 8 2010 Elazığ-Kovancılar earthquake. Nat Hazards 2012;61(2):703–17. https://doi.org/10.1007/s11069-011-0056-6.
[12] Celep Z, Erken A, Taskin B, Ilki A. Failures of masonry and concrete buildings during the March 8 2010 Kovancılar and Palu (Elazığ) earthquakes in Turkey. Eng Fail Anal 2011;18(1):868–89. https://doi.org/10.1016/j.engfailanal.2010.11.001.
[13] Inel M, Ozmen HB, Akyol E. Observations on the building damages after 19 May 2011 Simav (Turkey) earthquake. Bull Earthq Eng 2013;11(255):255–83. https://doi.org/10.1007/s10518-012-9414-3.
[14] Kocaman. İ. Damage mechanisms of masonry structures: an observation after 19 November Erzurum-Köprüköy Earthquake. J Struct Eng Appl Mech 2023;6(5):455–67. https://doi.org/10.31462/jseam.2023.05455467.
[15] Mercimek Ö. Seismic failure modes of masonry structures exposed to Kahramanmaraş Earthquakes (Mw 7.7 and 7.6) on February 6, 2023. Eng Fail Anal 2023;151:107422. https://doi.org/10.1016/j.engfailanal.2023.107422.
[16] Sayın E, Yön B, Calayır Y, Gör M. Construction failures of masonry and adobe buildings during the 2011 Van earthquakes in Turkey. Struct Eng Mech 2014;51(3):503–18. https://doi.org/10.12989/sem.2014.51.3.503.
[17] Sayın E, Yön B, Calayır Y, Karaton M. Failures of masonry and adobe buildings during the June 23 2011 Maden-(Elazığ) earthquake in Turkey. Eng Fail Anal 2013;34:779–91. https://doi.org/10.1016/j.engfailanal.2012.10.016.
[18] Ural A, Doğangün A, Sezen H, Angın Z. Seismic performance of masonry buildings during the 2007 Bala, Turkey earthquakes. Nat Hazards 2012;60:1013–26. https://doi.org/10.1007/s11069-011-9887-4.
[19] Yön B, Sayın E, Köksal TS. Seismic response of buildings during the May 19, 2011 Simav, Turkey earthquake. Earthq Struct 2013;5(3):343–57. https://doi.org/10.12989/eas.2013.5.3.343.
[20] Hafner I, Lazarević D, Kišiček T, Stepinac M. Post-earthquake assessment of a historical masonry building after the Zagreb earthquake—case study. Buildings 2022;12(3):323. https://doi.org/10.3390/buildings12030323.
[21] Rossetto T, Peiris N. Observations of damage due to the Kashmir earthquake of October 8, 2005 and study of current seismic provisions for buildings in Pakistan. Bull Earthq Eng 2009;7:681–99. https://doi.org/10.1007/s10518-009-9118-5.
[22] Zhao B, Taucer F, Rossetto T. Field investigation on the performance of building structures during the 12 May 2008 Wenchuan earthquake in China. Eng Struct 2009;31(1):1707–23. https://doi.org/10.1016/j.engstruct.2009.02.039.
[23] Tomassetti U, Correia AA, Graziotti F, Penna A. Seismic vulnerability of roof systems combining URM gable walls and timber diaphragms. Earthq Eng Struct Dyn 2019;48:1297–318. https://doi.org/10.1002/eqe.3187.
[24] Griffith MC, Lam NTK, Wilson JL, Doherty K. Experimental investigation of unreinforced brick masonry walls in flexure. J Struct Eng 2004;130:423–32. https://doi.org/10.1061/(ASCE)0733-9445(2004)130:3(423).
[25] Penner O, Elwood KJ. Out-of-plane dynamic stability of unreinforced masonry walls in one-way bending: shake table testing. Earthq Spectra 2016;32:1675–97. https://doi.org/10.1193/011415EQS009M.
[26] Giaretton M, Dizhur D, Ingham JM. Dynamic testing of as-built clay brick unreinforced masonry parapets. Eng Struct 2016;127:676–85. https://doi.org/10.1016/j.engstruct.2016.09.016.
[27] Graziotti F, Tomassetti U, Penna A, Magenes G. Out-of-plane shaking table tests on URM single leaf and cavity walls. Eng Struct 2016;125:455–70. https://doi.org/10.1016/j.engstruct.2016.07.011.
[28] Graziotti F, Tomassetti U, Sharma S, Grottoli L, Magenes G. Experimental response of URM single leaf and cavity walls in out-of-plane two-way bending generated by seismic excitation. Constr Build Mater 2019;195:650–70. https://doi.org/10.1016/j.conbuildmat.2018.10.076.
[29] Sharma S, Tomassetti U, Grottoli L, Graziotti F. Two-way bending experimental response of URM walls subjected to combined horizontal and vertical seismic excitation. Eng Struct 2020;219:110537. https://doi.org/10.1016/j.engstruct.2020.110537.
[30] Tomassetti U, Grottoli L, Sharma S, Graziotti F. Dataset from dynamic shake-table testing of five full-scale single leaf and cavity URM walls subjected to out-of-plane

two-way bending. Data Brief 2019;24:103854. https://doi.org/10.1016/j.dib.2019.103854.
[31] Sharma S, Grottoli L, Tomassetti U, Graziotti F. Dataset from shake-table testing of four full-scale URM walls in a two-way bending configuration subjected to combined out-of-plane horizontal and vertical excitation. Data Brief 2020;31:105851. https://doi.org/10.1016/j.dib.2020.105851.
[32] Landi L, Gabellieri R, Diotallevi PP. A model for the out-of-plane dynamic analysis of unreinforced masonry walls in buildings with flexible diaphragms. Soil Dyn Earthq Eng 2015;79:211–22. https://doi.org/10.1016/j.soildyn.2015.09.013.
[33] Penner O, Elwood KJ. Out-of-Plane Dynamic Stability of Unreinforced Masonry Walls in One-Way Bending: Parametric Study and Assessment Guidelines. Earthq Spectra 2016;32(3):1699–723. https://doi.org/10.1193/011715EQS011M.
[34] Derakhshan H, Griffith MC, Ingham JM. Out-of-plane seismic response of vertically spanning URM walls connected to flexible diaphragms. Earthq Eng Struct Dyn 2015;45(4):563–80. https://doi.org/10.1002/eqe.2671.
[35] Tondelli M, Beyer K, DeJong M. Influence of boundary conditions on the out-of-plane response of brick masonry walls in buildings with RC slabs. Earthq Eng Struct Dyn 2016;45(8):1337–56. https://doi.org/10.1002/eqe.2710.
[36] Godio M, Beyer K. Quantifying the out-of-plane response of unreinforced masonry walls subjected to relative support motion. Frat Ed Integrità Strutt 2019;(50):194–208. https://doi.org/10.3221/IGF-ESIS.50.17.
[37] Candeias PX, Costa AC, Mendes N, Costa AA, Lourenço PB. Experimental Assessment of the Out-of-Plane Performance of Masonry Buildings Through Shaking Table Tests. Int J Arch Herit 2017;11:31–58. https://doi.org/10.1080/15583058.2016.1238975.
[38] Magenes G, Penna A, Senaldi IE, Rota M, Galasco A. Shaking table test of a strengthened full-scale stone masonry building with flexible diaphragms. Int J Arch Herit 2014;8:349–75. https://doi.org/10.1080/15583058.2013.826299.
[39] Guerrini G, Senaldi I, Graziotti F, Magenes G, Beyer K, Penna A. Shake-table test of a strengthened stone masonry building aggregate with flexible diaphragms. Int J Arch Herit 2019;13:1078–97. https://doi.org/10.1080/15583058.2019.1635661.
[40] Graziotti F, Tomassetti U, Kallioras S, Penna A, Magenes G. Shaking table test on a full scale URM cavity wall building. Bull Earthq Eng 2017;15:5329–64. https://doi.org/10.1007/s10518-017-0185-8.
[41] Kallioras S, Graziotti F, Penna A, Magenes G. Effects of vertical ground motions on the dynamic response of URM structures: Comparative shake-table tests. Earthq Eng Struct Dyn 2022;51:347–68. https://doi.org/10.1002/eqe.3569.
[42] Miglietta M, Damiani N, Guerrini G, Graziotti F. Full-scale shake-table tests on two unreinforced masonry cavity-wall buildings: effect of an innovative timber retrofit. Bull Earthq Eng 2021;19:2561–96. https://doi.org/10.1007/s10518-021-01057-5.
[43] Kallioras S, Correia AA, Graziotti F, Penna A, Magenes G. Collapse shake-table testing of a clay-URM building with chimneys. Bull Earthq Eng 2020;18:1009–48. https://doi.org/10.1007/s10518-019-00730-0.
[44] Tomassetti U, Correia AA, Candeias PX, Graziotti F, Campos Costa A. Two-way bending out-of-plane collapse of a full-scale URM building tested on a shake table. Bull Earthq Eng 2019;17:2165–98. https://doi.org/10.1007/s10518-018-0507-5.
[45] Mirra M, Ravenshorst G. Optimizing seismic capacity of existing masonry buildings by retrofitting timber floors: wood-based solutions as dissipative alternative to rigid concrete diaphragms. Buildings 2021;11(12):604. https://doi.org/10.3390/buildings11120604.
[46] Mirdad MAH, Daneshvar H, Joyce T, Chui YH. Sustainability design considerations for timber-concrete composite floor systems. Adv Civ Eng 2021;2021:1–11. https://doi.org/10.1155/2021/6688076.
[47] Damiani N, Guerrini G, Graziotti F. Design procedure for a timber-based seismic retrofit applied to masonry buildings. Eng Struct 2024;301:116991. https://doi.org/10.1016/j.engstruct.2023.116991.
[48] Guerrini G, Damiani N, Miglietta M, Graziotti F. Experimental validation of analytical equations for retrofitting masonry buildings with timber frames and boards. Eng Struct 2024;300:117124. https://doi.org/10.1016/j.engstruct.2023.117124.
[49] Mirra M, Ravenshorst G, de Vries P, Messali F. Experimental characterisation of as-built and retrofitted timber-masonry connections under monotonic, cyclic and dynamic loading. Constr Build Mater 2022;358:129446. https://doi.org/10.1016/j.conbuildmat.2022.129446.
[50] Gubana A, Melotto M. Experimental tests on wood-based in-plane strengthening solutions for the seismic retrofit of traditional timber floors. Constr Build Mater 2018;191:290–9. https://doi.org/10.1016/j.conbuildmat.2018.09.177.
[51] Branco JM, Kekeliak M, Lourenço PB. In-plane stiffness of timber floors strengthened with CLT. Eur J Wood Wood Prod 2015;73:313–23. https://doi.org/10.1007/s00107-015-0892-2.
[52] Brignola A, Pampanin S, Podestà S. Experimental Evaluation of the In-Plane Stiffness of Timber Diaphragms. Earthq Spectra 2012;28:1687–709. https://doi.org/10.1193/1.4000088.
[53] Giongo I, Dizhur D, Tomasi R, Ingham JM. In-plane assessment of existing timber diaphragms in URM buildings via quasi-static and dynamic in-situ testing. Adv Mat Res 2013;778:495–502. https://doi.org/10.4028/www.scientific.net/AMR.778.495.
[54] Wilson A, Quenneville PJH, Ingham JM. In-plane orthotropic behavior of timber floor diaphragms in unreinforced masonry buildings. J Struct Eng 2014;140. https://doi.org/10.1061/(ASCE)ST.1943-541X.0000819.
[55] Peralta DF, Bracci JM, Hueste MBD. Seismic behavior of wood diaphragms in pre-1950s unreinforced masonry buildings. J Struct Eng 2004;130:2040–50. https://doi.org/10.1061/(ASCE)0733-9445(2004)130:12(2040).
[56] Mirra M, Ravenshorst G, van de Kuilen J-W. Experimental and analytical evaluation of the in-plane behaviour of as-built and strengthened traditional wooden floors. Eng Struct 2020;211:110432. https://doi.org/10.1016/j.engstruct.2020.110432.
[57] Giuriani E, Marini A. Wooden roof box structure for the anti-seismic strengthening of historic buildings. Int J Arch Herit 2008;2:226–46. https://doi.org/10.1080/15583050802063733.
[58] Mirra M, Gerardini A, Ghirardelli S, Ravenshorst G, van de Kuilen JW. Combining architectural conservation and seismic strengthening in the wood-based retrofitting of a monumental timber roof: the case study of St. Andrew's Church in Ceto, Brescia, Italy. Int J Arch Herit 2023;18(5):750–70. https://doi.org/10.1080/15583058.2023.2187726.
[59] Mirra M, Gerardini A, Ravenshorst G. Application of timber-based techniques for seismic retrofit and architectural restoration of a wooden roof in a stone masonry church. Procedia Struct Integr 2023;44:1856–63. https://doi.org/10.1016/j.prostr.2023.01.237.
[60] Mirra M, Gerardini A. Structural Upgrading and Architectural Conservation of a Historic Timber and Masonry Venetian Sawmill. In: Mazzolani FM, Landolfo R, Faggiano B, editors. Protection of Historical Constructions. PROHITECH 2025. Lecture Notes in Civil Engineering, 596. Cham: Springer; 2025. https://doi.org/10.1007/978-3-031-87316-4_62.
[61] Rizzi E, Capovilla M, Piazza M, Giongo I. In-plane behaviour of timber diaphragms retrofitted with CLT panels. Chapter in book. In: Aguilar R, et al., editors. Structural Analysis of Historical Constructions, 18. RILEM Bookseries; 2019. p. 1613–22. https://doi.org/10.1007/978-3-319-99441-3_173.
[62] Longarini N, Crespi P, Zucca M. The influence of the geometrical features on the seismic response of historical churches reinforced by different cross lam roof-solutions. Bull Earthq Eng 2022;20:6813–52. https://doi.org/10.1007/s10518-022-01468-y.
[63] ⟨https://www.tudelft.nl/citg/over-faculteit/afdelingen/materials-mechanics-management-design-3md/sections-labs/applied-mechanics/structural-mechanics/research/eries-supreme⟩ (project website). URL last seen on 30th April 2025.
[64] Damiani N, Graziotti F, Messali F, Sharma S. Out-of-plane shake-table tests on full-scale urm gables considering different roof configurations (ERIES-SUPREME). Built Environ Data Pavia Italy 2024. https://doi.org/10.60756/euc-1avy7q49.
[65] Sharma S, Damiani N, Bertassi M, Smerilli M, Mirra M, Lanese I, Rizzo Parisi E, O'Reilly G, Messali F, Graziotti F. Experimental data from out-of-plane shake-table tests on unreinforced masonry gables. Earthq Spectra 2025 (forthcoming).
[66] ⟨https://www.eucentre.it/laboratories-eucentre/experimental-laboratories/?lang=en⟩. URL last seen on 30th April 2025.
[67] Shabani A, Zucconi M, Kazemian Kioumarsi M. Seismic fragility analysis of low-rise unreinforced masonry buildings subjected to near- and far-field ground motions. Results Eng 2023;18:101221. https://doi.org/10.1016/j.rineng.2023.101221.
[68] Diaferio M, Foti D. Mechanical behavior of buildings subjected to impulsive motions. Bull Earthq Eng 2016;14:849–62. https://doi.org/10.1007/s10518-015-9848-5.
[69] Dolce M, Nicoletti M, De Sortis A, Marchesini S, Spina D, Talanas F. Osservatorio sismico delle strutture: the Italian structural seismic monitoring network. Bull Earthq Eng 2017;15:621–41. https://doi.org/10.1007/s10518-015-9738-x.
[70] Cattari S., Degli Abbati S., Ottonelli D., Marano C., Camata G., Spacone E., da Porto F., Modena C., Lorenzoni F., Magenes G., Penna A., Graziotti F., Ceravolo R., Miraglia G., Lenticchia E., Fiorini N., Spina D. Discussion on data recorded by the Italian structural seismic monitoring network on three masonry structures hit by the 2016-2017 Central Italy earthquake. 7th ECCOMAS Thematic Conference on Computational Methods in Structural Dynamics and Earthquake Engineering, Crete, Greece, 24-26 June 2019. https://doi.org/10.7712/120119.7044.20004.
[71] Bommer JJ, Stafford PJ, Edwards B, Dost B, van Dedem E, Rodriguez-Marek A, Kruiver P, van Elk J, Doornhof D, Ntinalexis M. Framework for a ground-motion model for induced seismic hazard and risk analysis in the groningen gas field, The Netherlands. Earthq Spectra 2017;33(2):481–98. https://doi.org/10.1193/082916EQS138M.
[72] van Elk J, Doornhof D, Bommer JJ, Bourne SJ, Oates SJ, Pinho R, Crowley H. Hazard and risk assessments for induced seismicity in Groningen. Neth J Geosci 2017;95(5):s259–69. https://doi.org/10.1017/njg.2017.37.
[73] Bommer JJ, Stafford PJ, Ruigrok E, Rodriguez-Marek A, Ntinalexis M, Kruiver PP, Edwards B, Dost B, van Elk J. Ground-motion prediction models for induced earthquakes in the Groningen gas field, the Netherlands. J Seismol 2022;26:1157–84. https://doi.org/10.1007/s10950-022-10120-w.
[74] NPR 9998:2020. Assessment of the structural safety of buildings in case of erection, reconstruction, and disapproval – Induced earthquakes – Basis of design, actions and resistances. Royal Netherlands Standardization Institute (NEN).
[75] Webtool NPR 9998: Bepaling van de seismische belasting. ⟨https://seismischekrachten.nen.nl/⟩. Royal Netherlands Standardization Institute (NEN). URL last seen on 30th September 2024.
[76] Graziotti F, Penna A, Magenes G. A comprehensive in situ and laboratory testing programme supporting seismic risk analysis of URM buildings subjected to induced earthquakes. Bull Earthq Eng 2019;17:4575–99. https://doi.org/10.1007/s10518-018-0478-6.
[77] Messali F, Longo M, Singla A, Rots JG. A comparative computational study on the static pushover and dynamic time history response of a masonry building (Meschke, Pichler & Rots (Eds)) Comput Model Concr Concr Struct 2022. https://doi.org/10.1201/9781003316404-41 (Meschke, Pichler & Rots (Eds)).

[78] Lagomarsino S, Penna A, Galasco A, Cattari S. TREMURI program: an equivalent frame model for the nonlinear seismic analysis of masonry buildings. Eng Struct 2013;56:1787–99. https://doi.org/10.1016/j.engstruct.2013.08.002.
[79] D'Altri AM, Messali F, Rots J, Castellazzi G, de Miranda S. A damaging block-based model for the analysis of the cyclic behaviour of full-scale masonry structures. Eng Fract Mech 2019;209:423–48. https://doi.org/10.1016/j.engfracmech.2018.11.046.
[80] Lourenço PB, Rots JG. Multisurface interface model for analysis of masonry structures. J Eng Mech 1997;123(7). https://doi.org/10.1061/(ASCE)0733-9399(1997)123:7(660).
[81] Casolo S. Modelling in-plane micro-structure of masonry walls by rigid elements. Int J Solids Struct 2004;41(13):3625–41. https://doi.org/10.1016/j.ijsolstr.2004.02.002.
[82] Sharma S, Silva LC, Graziotti F, Magenes G, Milani G. Modelling the experimental seismic out-of-plane two-way bending response of unreinforced periodic masonry panels using a non-linear discrete homogenized strategy. Eng Struct 2021;242:112524. https://doi.org/10.1016/j.engstruct.2021.112524.
[83] Sharma S, Marasca A, Ponte M, Bento R. Modelling the in-plane cyclic behaviour of typical Portuguese rubble stone masonry using the applied element method. Structures 2022;46:1224–42. https://doi.org/10.1016/j.istruc.2022.10.107.
[84] Oktiovan YP, Messali F, Pulatsu B, Lemos JV, Rots JG. A contact-based constitutive model for the numerical analysis of masonry structures using the distinct element method. Comput Struct 2024;303:107499. https://doi.org/10.1016/j.compstruc.2024.107499.
[85] Malomo D, Pinho R, Penna A. Numerical modelling of the out-of-plane response of full-scale brick masonry prototypes subjected to incremental dynamic shake-table tests. Eng Struct 2020;209:110298. https://doi.org/10.1016/j.engstruct.2020.110298.
[86] Kallioras S, Graziotti F, Penna A. Numerical assessment of the dynamic response of a URM terraced house exposed to induced seismicity. Bull Earthq Eng 2019;17:1521–52. https://doi.org/10.1007/s10518-018-0495-5.
[87] Fusco D, Addessi D, Messali F, Rots JG, Pampanin S. An analytical and numerical approach for shear failure of pier-wall connectionsin typical dutch URM buildings. Int J Arch Herit 2023;17(1):170–89. https://doi.org/10.1080/15583058.2022.2122762.
[88] Morandini C, Malomo D, Pinho R, Penna A. Development and validation of a numerical strategy for the seismic assessment of a timber retrofitting solution for URM cavity-wall buildings. Int J Arch Herit 2023;27(8):2224–43. https://doi.org/10.1080/13632469.2022.2104960.
[89] Damiani N, DeJong MJ, Albanesi L, Penna A, Morandi P. Distinct element modeling of the in-plane response of a steel-framed retrofit solution for URM structures. Earthq Eng Struct Dyn 2023;52(10):3030–52. https://doi.org/10.1002/eqe.3910.
[90] ⟨https://manuals.dianafea.com/d106/Diana.html⟩. URL last seen on 30th September 2024.
[91] Rots JG, Messali F, Esposito R, Jafari S, Mariani V. Thematic keynote computational modelling of masonry with a view to Groningen induced seismicity. In Structural Analysis of Historical Constructions: Anamnesis, Diagnosis, Therapy, Controls. CRC Press; 2016. p. 227–38. https://doi.org/10.1201/9781315616995-29.
[92] ⟨https://manuals.dianafea.com/d107/en/1181807-1182186-engineering-masonry-model.html⟩. URL last seen on 30th September 2024.
[93] Skroumpelou G., Messali F., Esposito R., Rots J.G. Mechanical characterisation of wall tie connection in cavity walls. *10th Australasian Masonry Conference*, 11–14 February, 2018, Sydney, Australia.
[94] Arlsan O, Messali F, Smyrou E, Bal İE, Rots JG. Experimental characterization of the axial behavior of traditional masonry wall metal tie connections in cavity walls. Constr Build Mater 2021;266(A):121141. https://doi.org/10.1016/j.conbuildmat.2020.121141.
[95] Messali F, Longo M. Calibration of a mechanism-based method against NLFEA for NLPO analyses of URM terraced house units: Cross-validation and calibration of simplified methods for different building typologies. Report no. TC19/20-R01, Version 01. Delft University of Technology; 2019. ⟨https://pure.tudelft.nl/ws/portalfiles/portal/98471648/TC1920_R01_Cross_validation_SLaMA_FEM_URM_Terraced_houses_final.pdf⟩. Report no. TC19/20-R01, Version 01.
[96] Messali F., Longo M., Tavus A., Singla A. Calibration of a mechanism-based method against finite element analyses for the pushover analyses of low-rise masonry buildings. *Proceedings of the 8th International Conference on Computational Methods in Structural Dynamics and Earthquake Engineering* (COMPDYN 2021). Athens, Greece, 2021.
[97] Mirra M, Ravenshorst G, de Vries P, van de Kuilen JW. An analytical model describing the in-plane behaviour of timber diaphragms strengthened with plywood panels. Eng Struct 2021;235:112128. https://doi.org/10.1016/j.engstruct.2021.112128.
[98] Mirra M. A set of calculation tools supporting the design, modelling and application of plywood-based seismic retrofitting interventions on timber floors in existing buildings. Structures 2024;63:106378. https://doi.org/10.1016/j.istruc.2024.106378.
[99] Green RA, Bommer JJ, Stafford PJ, Maurer BW, Kruiver PP, Edwards B, Rodriguez-Marek A, de Lange G, Oates SJ, Storck T, Omidi P, Bourne SJ, van Elk J. Liquefaction hazard in the Groningen region of the Netherlands due to induced seismicity. J Geotech Geoenviron Eng 2020;146(8):04020068. https://doi.org/10.1061/(ASCE)GT.1943-5606.0002286.
[100] Graziotti F., Toninelli P., Solenghi M., Guerrini G., Penna A. Numerical simulation of the nonlinear earthquake response of a monitored URM school building. *Proceedings of the 7th International Conference on Computational Methods in Structural Dynamics and Earthquake Engineering* (COMPDYN 2019), Vol. 1, pp. 1827-1838. Crete, Greece, 2019. https://doi.org/10.7712/120119.7039.19171.
[101] Graziotti, F., Solenghi, M., Guerrini, G., & Penna, A. Macroelement modelling of a monitored URM school building accounting for seismic damage accumulation. *Proceedings of the XVIII ANIDIS Conference*, Ascoli Piceno, Italy, 2019. https://doi.org/10.1400/271243.